Journal of Hydrology: Regional Studies 36 (2021) 100847

Contents lists available at ScienceDirect

Journal of Hydrology: Regional Studies

journal homepage: www.elsevier.com/locate/ejrh

Application of the Least-Squares Wavelet software in hydrology: Athabasca River Basin

Ebrahim Ghaderpour [a,b,*], Tijana Vujadinovic [b], Quazi K. Hassan [a]

[a] Department of Geomatics Engineering, University of Calgary, 2500 University Drive NW, Calgary, AB T2N 1N4, Canada
[b] Earth and Space Inc., Calgary, AB, Canada

ARTICLE INFO

Keywords:
Climate change
Coherency analysis
Data gaps
Spectral analysis
Trend analysis
Water flow analysis

ABSTRACT

Study region: Athabasca River Basin (ARB) in Alberta, Canada.
Study focus: Understanding the historical streamflow variability within basins is crucial to reduce the effect of utmost events, such as drought and floods on agriculture, fishery, and other human activities. The Least-Squares Wavelet software (LSWAVE) is applied to estimate the trend and seasonal components of sixty-year-long climate and discharge time series and to study the impact of climate change on streamflow over time.
New hydrological insights for the region: The seasonal components of the discharge and precipitation time series including annual and semi-annual are coherent with phase discrepancy. The mean temperature has been gradually increasing since 1960, and it is projected to increase by approximately 2 °C during the mid-century which may reduce the snowpack volume during the spring. From the recurring pattern of spectral peaks in the spectrograms and jumps in the trend component of streamflow time series, the blue water is projected to increase during the mid-century, in particular in early 2030s. The results also highlight the potential of LSWAVE in analyzing climate and hydrological time series without any need for interpolation, gap-filling, and de-spiking.

1. Introduction

An understanding of spatial and temporal variability of streamflow and its relationship with climate change in a region not only can enhance our hydrological and ecological knowledge but it can also help to improve forecasting and reducing the impact of extreme events, including floods and drought within the region on human activities (Payne et al., 2004; Schultea et al., 2016; Eum et al., 2017). There are many challenges in hydrological processes most of which arise from the quality and quantity of measurements and uncertainties in the measurements. Furthermore, climate and hydrological data often contain inter- and intra-annual variations that must be considered when studying both short- and long-term changes within a region.

A time series is a sequence of measurements (observations) recorded over time (time-indexed). Time series in many practical applications are not sampled at equally spaced time intervals (unequally spaced) and may have associated covariance matrices that contain the variances of measurements and the co-variances between the measurements. Vaníček (1969) proposed the Least-Squares Spectral Analysis (LSSA) to analyze unequally spaced time series in the frequency domain. Unlike the Fourier transform, LSSA can analyze unequally spaced time series and can consider the associated covariance matrices (Craymer, 1998; Mallat, 1999). The

* Corresponding author.
E-mail addresses: ebrahim.ghaderpour@ucalgary.ca (E. Ghaderpour), info@earthspace.ca (T. Vujadinovic), qhassan@ucalgary.ca (Q.K. Hassan).

https://doi.org/10.1016/j.ejrh.2021.100847
Received 9 December 2020; Received in revised form 13 May 2021; Accepted 7 June 2021
Available online 30 June 2021

Anti-Leakage Least-Squares Spectral Analysis (ALLSSA) is an improved version of LSSA that uses the original data to iteratively decide whether there are any statistically significant components in the time series. Thus, ALLSSA finds an optimal series of functions (e.g., sinusoids and trends) that simultaneously fit best to the time series which can prevent over/under-fitting problems, like the least absolute shrinkage and selection operator (Tibshirani, 1996; Zhu et al., 2015). For regularization and forecasting purposes, ALLSSA performs better than the ordinary least-squares method (Ghaderpour et al., 2018b; Ghaderpour and Vujadinovic, 2020a,b).

The relationship between climate change and streamflow is not straightforward. The climate and streamflow time series usually contain inter- and intra-annual components that can be scrutinized in the time-frequency domain. Wavelet analysis is a robust approach for investigating whether such components exist and how they are varying over time. The Continuous Wavelet Transform (CWT) transforms an equally spaced time series (without gaps and missing values) into the time-scale or time-frequency domain and obtains a scalogram or a spectrogram, respectively (Torrence and Compo, 1998; Mallat, 1999). The Cross Wavelet Transform (XWT) is also based on CWT proposed for the sake of analyzing two non-stationary time series together in the time-scale or time-frequency domain (Torrence and Compo, 1998; Grinsted et al., 2004). The time series in XWT must however be equally spaced with the same time distributions (same sampling rates). CWT and XWT are widely used to analyze climate and hydrological time series (Labat, 2008; Schultea et al., 2016; Azuara et al., 2020; Liu et al., 2020). For example, Labat (2008) and Schultea et al. (2016) applied CWT (using the Morlet wavelet) and found annual and intra-annual components in the streamflow time series of rivers across the Mid-Atlantic region, and they further investigated the impact of climate on streamflow via XWT. Other wavelet analyses are also increasingly used in hydrology, such as wavelet coherence analysis (Graf et al., 2014; Fang et al., 2015) and the Hilbert-Huang transform (Rudi et al., 2010).

On the other hand, the Least-Squares Wavelet Analysis (LSWA) and the Least-Squares Cross-Wavelet Analysis (LSCWA), natural extensions of LSSA, decompose the time series into the time-frequency domain and can be directly applied to any type of time series, i.e., the time series do not have to be equally spaced and they can have any time distributions (Ghaderpour and Pagiatakis, 2017; Ghaderpour et al., 2018a). LSWA and LSCWA can also consider the covariance matrices associated with the time series and provide higher time-frequency resolution spectrograms and more accurate amplitude estimation as compared to CWT and XWT, see the Supplementary Materials and Ghaderpour (2018). LSSA, ALLSSA, LSWA, and LSCWA are the main tools in the Least-Squares Wavelet software (LSWAVE).[1] Ghaderpour and Pagiatakis (2019) describes LSWAVE in detail.

The Athabasca River Basin (ARB), one of the major watershed in Alberta and widely studied by many researchers (Bawden et al., 2014; Eum et al., 2017; Hwang et al., 2018; Du et al., 2019), is chosen herein to show how LSWAVE can be used to study the streamflow variability over several decades and to show how climate change may have impacted the streamflow. The streamflow simulation has successfully been implemented using process-based models. For example, Shrestha et al. (2017), Shrestha and Wang (2018) simulated the effects of climate change on streamflow, freshwater resources, and sediment using the Soil and Water Assessment Tool (SWAT) in ARB. Also, Dibike et al. (2018) investigated the snow response of the Athabasca watershed to projected climate using the Variable Infiltration Capacity (VIC) hydrologic model and statistically downscaled future climate data from a selected set of CMIP5 Global Climate Models (GCMs) forced with RCP 4.5 and 8.5 emissions scenarios.

The main goal of this research is to highlight the potential of LSWAVE in analyzing climate and hydrological time series as they are provided without any need for pre-processing including interpolation, gap-filling, and de-spiking. The gradual and seasonal changes in streamflow over time are rigorously investigated via LSWAVE applied to the streamflow data acquired at eight major hydrometric stations along the Athabasca River. From spatiotemporal analysis of climate data and recurring spectral patterns in the spectrograms, some projections for blue water resources and climate for the mid-century are made and compared with previous results. Furthermore, for the sake of comparisons and completeness, other popular and traditional methods, such as hydrographs, box plots, and flow-duration curves, are also described herein and applied to the climate and streamflow data sets.

2. Materials and methods

2.1. Study region

ARB is a region of approximately 150,000 km^2 which covers about 24% of Alberta's landmass, see Fig. 1 The Athabasca River, the longest undammed river in the Canadian prairies, begins at the Columbia Glacier in Jasper National Park and travels the region about 1300 km toward the northeast and flows through the Peace-Athabasca Delta into Lake Athabasca (Du et al., 2019). The range of basin elevation is from 185 m near Lake Athabasca to about 3700 m (above sea level) in the mountainous areas near Jasper (Bawden et al., 2014). The basin is divided into a series of subbasins as shown in Fig. 1. The Athabasca River passes the towns of Jasper, Hinton, Whitecourt, Athabasca, and Fort McMurray, where there are hydrological stations that have been continuously measuring the streamflow since the 1960s, see P1-P5 in Fig. 1. Approximately 82% of the region is forested and 9.5% is agricultural land (Du et al., 2019). Forestry, agriculture, tourism, oil and gas extraction, coal, and oil sand mining are the major activities in this region.

2.2. Data sets and pre-processing

The historical climate data, i.e., the daily-maximum and daily-minimum temperatures and daily-precipitation since 1960 within

[1] LSWAVE: https://www.ngs.noaa.gov/gps-toolbox/LSWAVE.htm Updates: https://github.com/Ghaderpour/LSWAVE-SignalProcessing/.

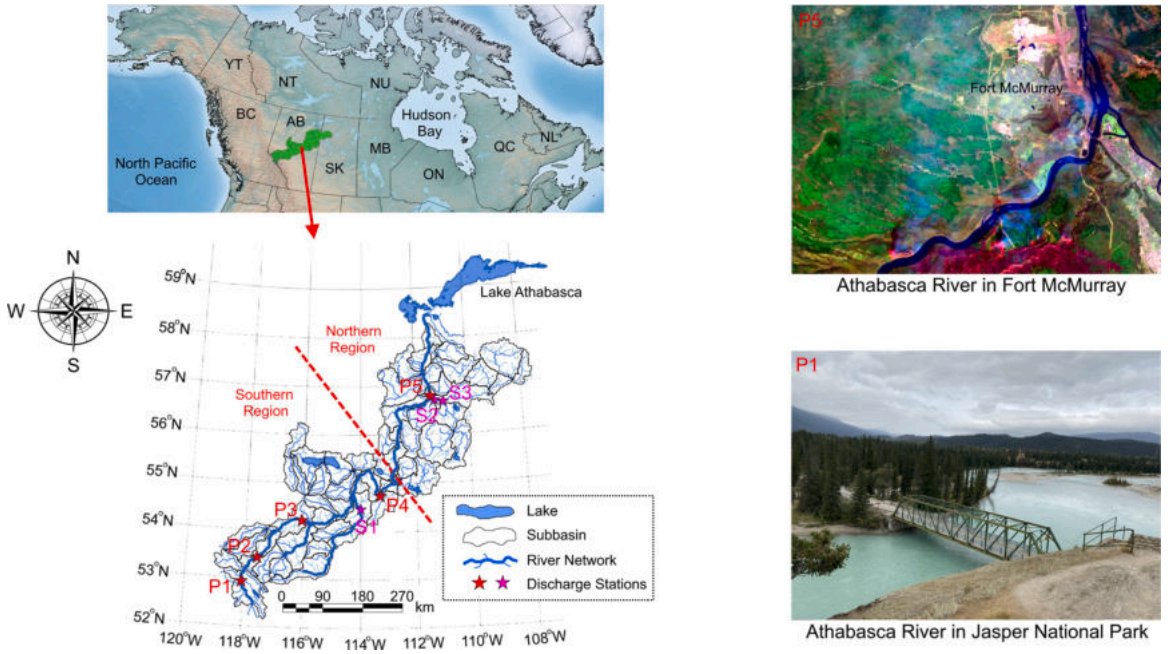

Fig. 1. ARB with eight hydrometric stations: five primary stations (P) along the Athabasca River and three secondary stations (S), where water is flowing to the Athabasca River, see also Table 1. The red dashed line divides the basin into the two regions. The top right panel is processed by the authors using Landsat-8 OLI images available from the U.S. Geological Survey. The bottom right photo is taken by T. Vujadinovic. (For interpretation of the references to color in this figure legend, the reader is referred to the web version of this article.)

Alberta, are provided by the Alberta Agriculture and Forestry, Government of Alberta.[2] The climate data have a spatial resolution of 0.1 degree in both latitude and longitude (townships), estimated by a mathematical data interpolation procedure that weighs up to several nearest station observations (Ruan et al., 2016; Eum and Gupta, 2019). Generally, the climate data are less reliable in the mountainous areas toward the southwest of the basin due to several factors, such as sparse observation network, topographic complexity, and orographic effects (Eum and Gupta, 2019). The geographic coordinates of the hydrological stations with their drainage areas and elevations are listed in Table 1.

The discharge data sets are provided by the Government of Canada.[3] Herein, five primary stations, denoted by letter P, and three secondary stations, denoted by letter S with continuous recorded measurements and relatively large drainage areas are analyzed. The discharge time series have many missing values and data gaps, in particular for P1, P2, P3, and S3. The data gaps are mostly during the winter period, from November to mid-April, due to several reasons, such as ice condition, backwater, equipment damage, and malfunctioning of the recording system (Kundzewicz and Robson, 2004; Slater and Villarini, 2016). The spectral and wavelet analyses performed herein leave the data gaps as they are without any need for gap-filling.

2.3. Methods

In this section, the traditional tools, such as box plots, hydrographs, and flow-duration curves are described first. Then, the least-squares spectral and wavelet analyses are briefly described, and the reader is referred to the Supplementary Materials for their mathematical details and some quantitative results.

2.3.1. Box plots

Box plots are frequently used for demonstrating basic statistics of data sets including their medians, quartiles, and outliers. A box plot conventionally uses five values from a data set: upper and lower extremes, upper and lower hinges (quartiles: the box edges), and the median (inside the box) (McGill et al., 1978). The outliers are data points located outside the whiskers of the box plot, i.e., data points whose values are beyond the extremes.

2.3.2. Hydrographs

Herein, hydrographs for a discharge time series are simply obtained as follows: (1) For monthly hydrographs over years, the monthly minimum, mean, and maximum of the discharge values are obtained for each year, (2) For each day of the year, the historical

[2] Climate data sets: https://agriculture.alberta.ca/acis.
[3] Streamflow data sets: https://wateroffice.ec.gc.ca/search/historical_e.html.

Table 1
The eight hydrometric stations shown in Fig. 1 along with their geographic coordinates, drainage areas, and elevations (above sea level).

Label	Station name	Latitude	Longitude	Drainage (km^2)	Elevation (m)
P1	Athabasca River near Jasper	52°54′37″	−118°03′31″	3,870	1059
P2	Athabasca River at Hinton	53°25′27″	−117°34′10″	9,760	954
P3	Athabasca River near Windfall	54°12′27″	−116°03′48″	19,600	736
P4	Athabasca River at Athabasca	54°43′19″	−113°17′17″	74,600	516
P5	Athabasca River below Fort McMurray	56°46′49″	−111°24′08″	133,000	237
S1	Pembina River at Jarvie	54°27′00″	−113°59′24″	13,100	609
S2	Clearwater River at Drapper	56°41′24″	−111°15′36″	30,800	261
S3	Clearwater River above Christina River	56°39′36″	−110°55′48″	18,061	271

minimum, mean, and maximum of the discharge values are obtained for that day since 1960. Thus, three graphs are obtained corresponding to the historical minimum, mean, and maximum discharge values, illustrated in one figure herein.

2.3.3. Flow-duration curve

Flow duration curve is another popular graphical tool that demonstrates the discharge that equaled or exceeded some percent of the time for a catchment or drainage area (Foster, 1934; Vogel and Fennessey, 1994). The time unit used in calculating a flow-duration curve affects its appearance. A commonly used time unit is the mean daily discharge (Li et al., 2010). Suppose that n is the total number of discharge daily values. First sort the daily discharge in descending order and then assign a rank λ ($1 \leq \lambda \leq n$) to each discharge value, starting with 1 for the largest daily discharge value. Finally, calculate the exceedance probability as follows:

$$P = \lambda/(n+1), \quad \lambda = 1, 2, \ldots, n, \tag{1}$$

which shows the probability that a given flow will be equaled or exceeded.

2.3.4. Least-Squares Spectral Analysis (LSSA)

LSSA obtains a frequency spectrum for a given time series which may not be equally spaced (Vaníček, 1969; Lomb, 1976). The spectrum is obtained by fitting the sinusoids to the entire time series without any need for pre-processing of the original measurements including interpolation, gap-filling, de-spiking, etc. (Craymer, 1998; Pagiatakis, 1999). The Anti-Leakage LSSA (ALLSSA) is an iterative method based on LSSA that finds an optimal set of sinusoids that along with the initial constituents (e.g., trends) simultaneously fit best the time series (Ghaderpour et al., 2018b). ALLSSA, compared to LSSA especially when the time series is unequally spaced, can therefore increase the accuracy of signal estimation as it simultaneously considers the correlation among the constituents of known forms and the sinusoidal functions of different frequencies that can be any real numbers. The Anti-Leakage Least-Squares Spectrum (ALLSS) shows the estimated amplitudes of statistically significant signals in the time series (Ghaderpour et al., 2018b).

2.3.5. Least-Squares Wavelet Analysis (LSWA)

LSWA is a natural extension of LSSA in that it decomposes the time series into the time-frequency domain rather than into the frequency domain (Ghaderpour and Pagiatakis, 2017). This allows the detection of both short- and long-duration signals with the variability of frequencies and amplitudes over time. In other words, the estimated amplitudes and phases of the time series components are localized in time and frequency neighborhoods, following the Heisenberg uncertainty principle like in CWT (Mallat, 1999, Chapter 1.3). LSWA segments the time series frequency-wise, i.e., as the frequency increases, the segment size decreases, and vice versa. Therefore, an amplitude and/or normalized spectrogram (LSWS) will be obtained which shows how the amplitude and/or percentage variance of the time series components change over time and frequency (Ghaderpour and Pagiatakis, 2017). Using a Gaussian function, one may assign higher weights to the observations toward the center of segments and lower weights to the observations toward both ends of the segment to mitigate the spectral leakages and smooth the spectral peaks in the spectrograms (Ghaderpour, 2018, Chapter 2.7). This selection for the weights will adapt the sinusoidal basis functions to the Morlet wavelet in the least-squares sense (Foster, 1996; Torrence and Compo, 1998).

2.3.6. Least-Squares Cross Wavelet Analysis (LSCWA)

LSCWA is a robust method of analyzing two time series together, e.g., discharge and precipitation time series, for investigating the coherency and phase differences between the components of both time series in the time-frequency domain like XWT (Grinsted et al., 2004; Ghaderpour et al., 2018a). Since the time distributions of the time series may not be the same, one may choose a common set of times for both time series (e.g., the union of the times in both time series) and compute a normalized spectrogram for each time series. The Least-Squares Cross-Wavelet Spectrogram (LSCWS) is defined by the product of the two spectrograms which shows the coherency of the components in percentage variance when multiplied by 100. If the values of LSCWS are closer to 100%, then the components of both series are highly coherent within the corresponding time-frequency neighborhoods, and they are incoherent for values closer to 0%. The phase differences in LSCWS show how much the components of the second time series lead/lag the ones in the first time series like in XWT. The phase difference is usually displayed by an arrow on LSCWS following the trigonometric circle principle. Thus, arrows pointing to the right and left mean the components are in-phase and out-of-phase, respectively (Ghaderpour et al., 2018a). Preferably, the arrows can be displayed only for the peaks in LSCWS whose percentage values are the highest among the values of neighboring

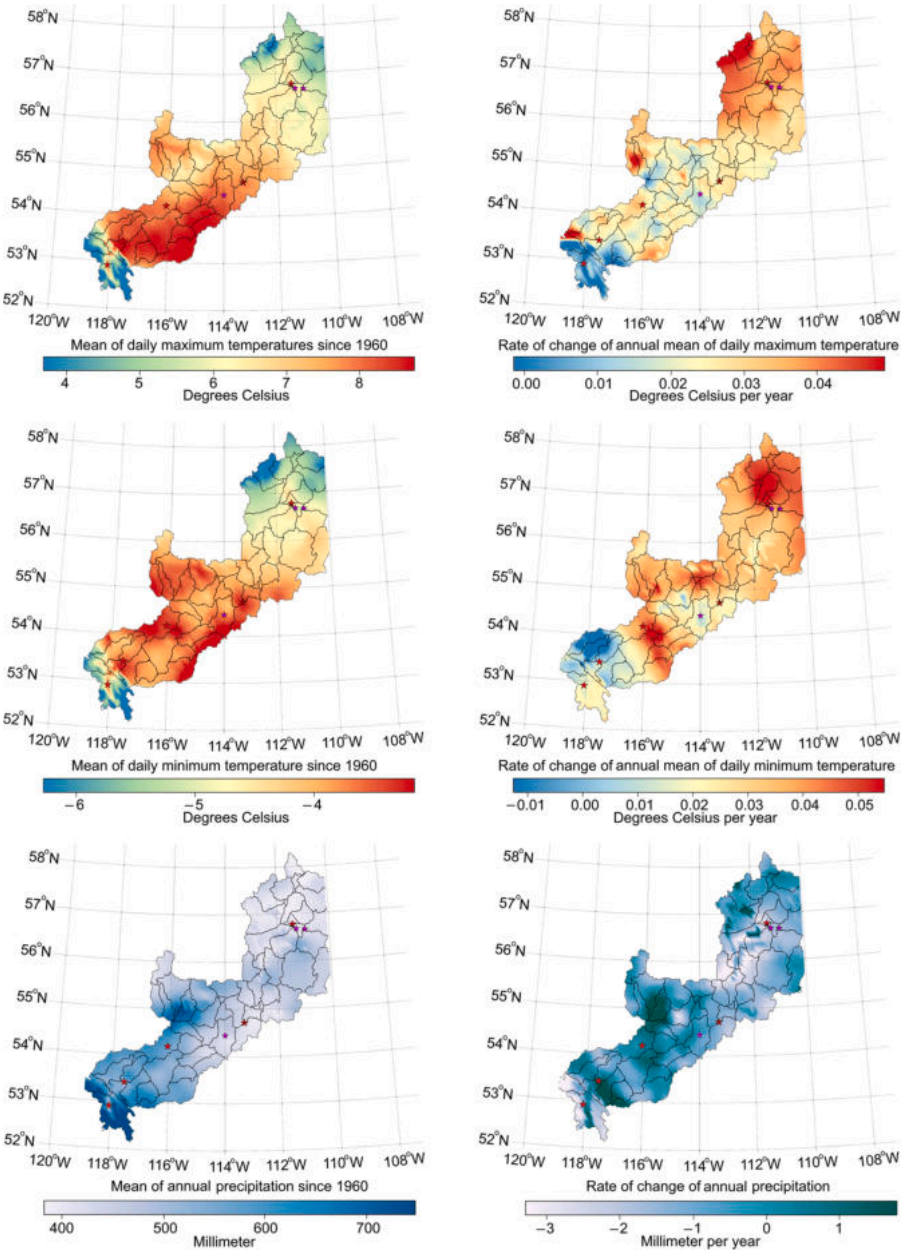

Fig. 2. Climate variation through ARB within Alberta's border derived from the gridded climate dataset available from the Government of Alberta https://agriculture.alberta.ca/acis/. Note that the derived product is not an official version of the materials reproduced, nor as having been made in affiliation with or with the endorsement of the Government of Alberta. Each panel includes the subbasins and hydrometric stations shown by stars.

peaks.

The Least-Squares Cross-Spectral Analysis (LSCSA) is a special case of LSCWA which multiplies the Least-Squares Spectra (LSSs) of both time series to obtain a cross-spectrum (LSCS), and no windowing strategy is applied. Therefore, LSCSA is not suitable for estimating the phase differences of unstable components over time as it averages them out, similarly for the signal estimation like LSSA vs. LSWA. Finally, the statistical properties of LSCWA and LSCSA follow from the normality assumption of time series like in LSSA and LSWA (Ghaderpour et al., 2018a).

2.3.7. Trend analysis

To investigate gradual changes over decades rather than an overall gradual change for the entire discharge time series, the Jumps Upon Spectrum and Trend (JUST) is also applied herein to find potential jumps in the trend component of the time series (Ghaderpour and Vujadinovic, 2020a). JUST applies an appropriate windowing (segmentation) technique to find an optimal set of jump locations in

the trend component of the time series. Herein, a window covering approximately a decade of data is selected that translates over time by four-year steps. Within each translating window, a linear trend with two pieces will be estimated that minimizes the residual norm, see Supplementary Section 1. Following this process, an optimal jump location for the linear trend within each window is estimated. Finally, only the jumps will be selected whose locations are closest to the window locations where they were estimated and are at least a decade apart from each other (Ghaderpour and Vujadinovic, 2020a). Ghaderpour (2021) describes the JUST software in detail, freely available online in both MATLAB and Python.[4]

The estimated daily climate data are used herein for equally spaced grids that are 0.1 degrees apart in both latitude and longitude within ARB and Alberta's border. For each spatial grid, the means of time series for the daily maximum and minimum temperatures and annual precipitation are calculated. Furthermore, for each spatial grid and each year since 1960, the average of daily maximum and daily minimum temperatures are calculated to obtain two time series of size sixty each. Similarly, the daily precipitations are added within each year to obtain an annual precipitation time series for each spatial grid. Then, JUST is applied to each time series of size sixty to estimate the overall linear trend for each of the annual mean of daily maximum and minimum temperature as well as for the annual precipitation time series. Therefore, six sets of spatial data points for the region within Alberta's border are obtained, where the value of each data point in a set is either the average climate value or the rate of change of climate values since 1960. Finally, the Triangulated Irregular Network (TIN) interpolation (Mitas and Mitasova, 1999), a popular method in Geographic Information System (GIS), is applied to generate the climate maps for ARB in this study.

3. Results

3.1. Climate data analyses

Figure 2 shows the climate variation results for ARB. Since the southwest part of the region near Jasper (P1) is by the rocky mountains, it is generally colder than the rest of the region with higher average annual precipitation (about 700 mm). The north part of the region (above Fort McMurray) is colder than the center of the region, and the trend analysis result shows that the north part is getting warmer at a faster rate compared to the central region since 1960. From the six sets of spatial data points (before the TIN interpolation), the maximum and minimum temperatures of 99% and 97% the region have been increasing by 0.029 and 0.034 °C/a on average, respectively. Moreover, the annual precipitation of 91% of the region has been decreasing by 1.56 mm/a since 1960.

To further investigate the temporal variability of climate data, the region within Alberta's border is divided into two sub-regions, namely, the southern and northern regions, using the red dashed line shown in Fig. 1. The historical monthly box plots of the daily-maximum and daily-minimum temperatures for the basin within Alberta's border, and the southern and northern regions are illustrated in Fig. 3. Furthermore, the monthly-accumulated precipitations are calculated and their corresponding historical box plots are shown in the bottom three panels of Fig. 3. The blue circles in these panels are the outliers, and the red solid lines inside the boxes are the medians of the historical data sets since 1960. From the box plots, one can observe that months of January and July are the coldest and warmest months for the region and sub-regions.

The trend, spectral, and wavelet analyses of the daily-maximum, daily-minimum, and daily-precipitation time series for the northern region are illustrated in Fig. 4. For the sake of brevity, such climate analyses are shown only for the northern region to show how one may investigate the impact of climate change on the streamflow using theses analyses. Herein, the northern region is chosen to investigate how the precipitation may have affected the flow near Fort McMurray (P5) with the highest drainage area (133,000 km^2) after the flow is measured at Athabasca (P4).

The estimated linear trends using the simple and simultaneous season-trend fit models are shown by the solid red and green lines in the time series panels in Fig. 4, respectively. From Table 2, one can see that the estimated intercepts and slopes of the linear trends are approximately the same using both models in these cases. The ALLSSA amplitude spectra whose estimated linear trends are shown by the solid green lines are illustrated in the left panels of Fig. 4. LSWSs representing the estimated amplitudes are shown under the time series panels. From LSWSs in Fig. 4a and b, both daily-maximum and daily-minimum temperature time series show almost stable dominant annual components over time (see the reddish horizontal band of spectra at one cycle/year). From Fig. 4c, LSWS shows annual and semi-annual components and many other short-duration higher frequency components with amplitude variability over time for the daily-precipitation series.

3.2. Streamflow analyses

The monthly hydrographs of the discharge time series since 1960 are shown in Fig. 5. From this figure, one can observe that the seasonal component of streamflow in ARB may be simulated by asymmetric Gaussian functions as demonstrated in the Supplementary Materials. The sixty-year hydrographs of the discharge time series since 1960 are also illustrated in Fig. 6. The maximum flows of more than 2000, 4000, 4500 m^3/s are observed in July at stations P3, P4, P5, respectively, see Fig. 6c, d, and e. The least overall streamflow is also observed in Fig. 6h (S3). Fig. 6d–h also show large peaks during April and May for the daily-maximum historical discharge.

Figure 7 shows the flow-duration curves of the discharge data measured at the eight stations. From the left panel in this figure, it can be seen that the probability that the flow at the Athabasca River below Fort McMurray exceeds 1000 m^3/s is 0.2 while at Athabasca is

[4] JUST: https://geodesy.noaa.gov/gps-toolbox/JUST.htm.

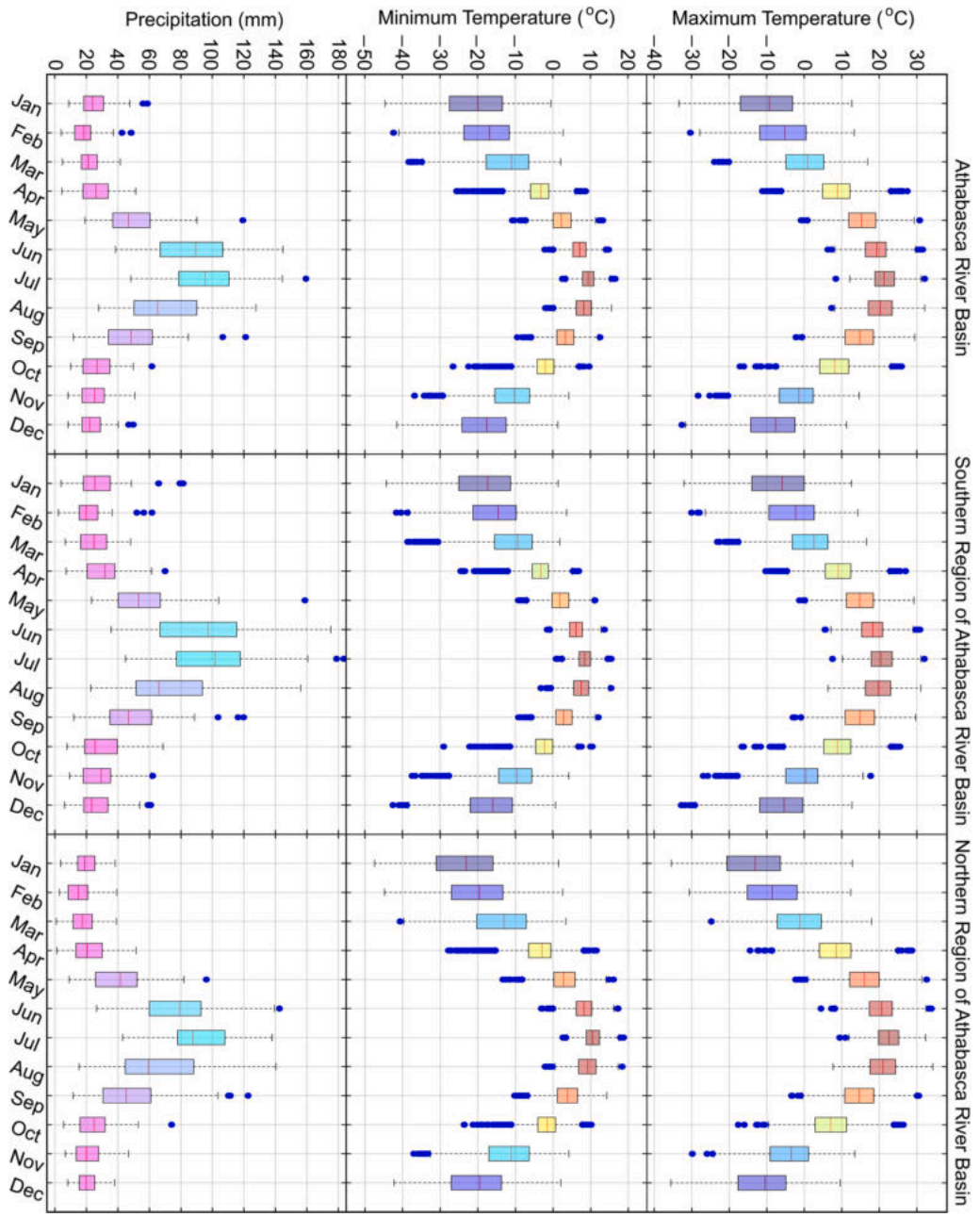

Fig. 3. The historical monthly box plots since 1960 for ARB and its southern and northern regions within Alberta's border: Top three panels for the maximum temperature (daily-maximum), middle three panels for the minimum temperature (daily-minimum), and bottom three panels for the precipitation (monthly-accumulated). (For interpretation of the references to color in the text, the reader is referred to the web version of this article.)

0.1, see the blue solid and black dashed lines. The right panel also shows that the probability that the flow at the Clearwater River above Christina River exceeds 100 m^3/s is 0.2 while with the same probability flow exceeds 50 m^3/s for the Pembina River at Jarvie, see the blue solid and red dashed lines. Furthermore, the flow in none of the curves in the right panel, corresponding to stations P1, S1, S2, and S3, exceeds 1000 m^3/s.

The box plots of the historical discharge data sets for the eight stations are shown in Fig. 8. The largest and smallest medians are for the discharge data sets corresponding to P5 (457 m^3/s) and S1 (14 m^3/s), respectively. The outliers are shown by the blue circles. From the box plots, one can observe that the discharge values generally increase from P1 to P5 mainly due to flowing water into the Athabasca River from other smaller streams and rivers, such as the Pembina River (S1) and Clearwater River (S2).

The daily discharge time series corresponding to each station along with the estimated linear trends using simple and simultaneous

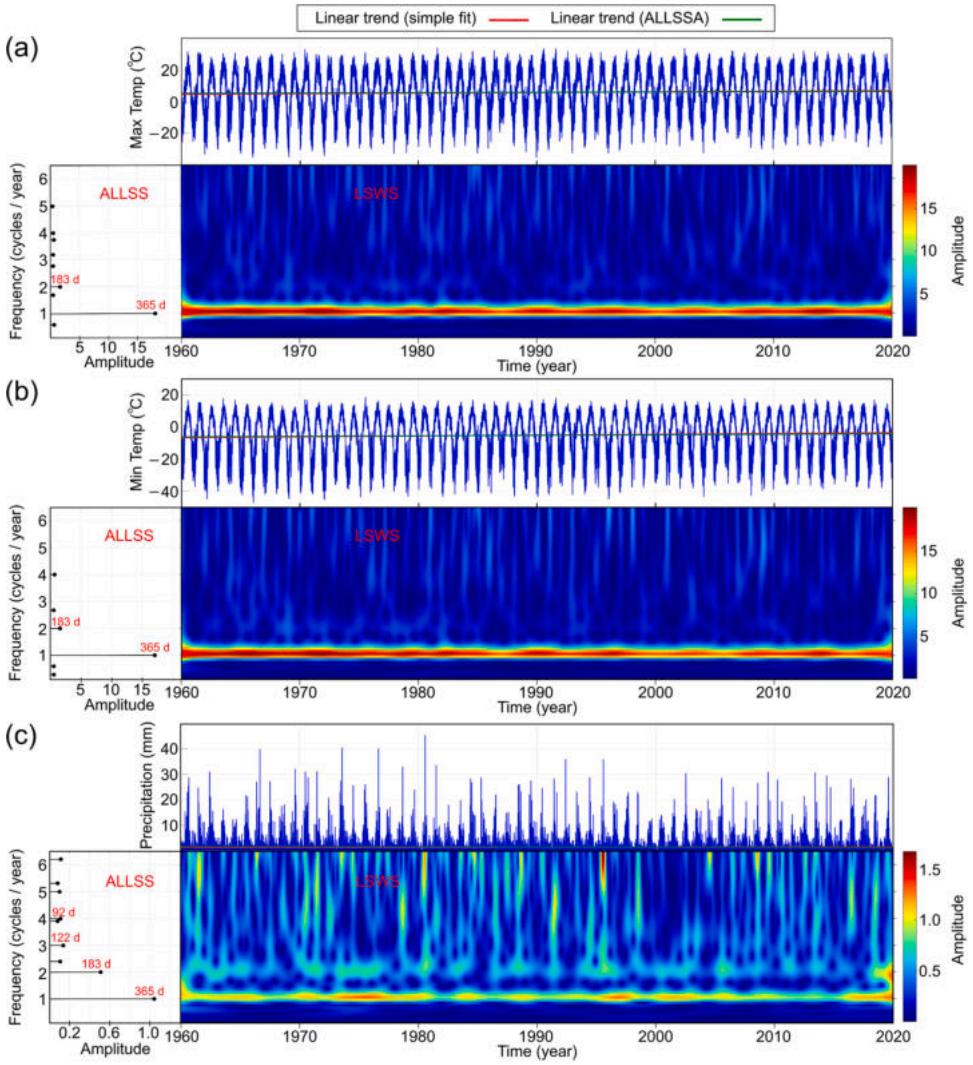

Fig. 4. Climate time series for the northern region of ARB within Alberta's border as shown in Fig. 1 along with the linear trend fits whose intercepts and slopes are listed in Table 2 and their corresponding ALLSSs and LSWSs. Note that there is no significant difference between the linear trends using the simple fit method and ALLSSA in this figure. (For interpretation of the references to color in the text, the reader is referred to the web version of this article.)

Table 2
The estimated intercepts and slopes of the linear trends for the climate series shown in Fig. 4. The rates (slopes) are the amounts per year.

Time series type (daily)	Intercept (simple fit)	Slope (simple fit)	Intercept (ALLSSA)	Slope (ALLSSA)
Max temperature (°C)	4.8891 ± 0.1942	0.0353 ± 0.0056	4.9496 ± 0.0869	0.0335 ± 0.0025
Min temperature (°C)	-6.3935 ± 0.1829	0.0425 ± 0.0053	-6.2830 ± 0.0819	0.0390 ± 0.0024
Precipitation (mm)	1.4160 ± 0.0365	-0.0043 ± 0.0011	1.4192 ± 0.0344	-0.0044 ± 0.0010

season-trend fit models are illustrated in blue, red, and green lines, respectively, in Figs. 9 and 10. The estimated intercepts and slopes of the linear trends via each model are listed in Table 3. The estimated intercepts and slopes using ALLSSA are more accurate with lower uncertainties (errors) as compared to the simple model, especially for unequally spaced time series. Considering the errors, these results are approximately the same for all the time series except for P3 and S3, see Figs. 9b and 10d. One of the main reasons that the slope difference is significant for P3 is the consistent data gaps during the winter since 1979, where the presumably smaller discharge

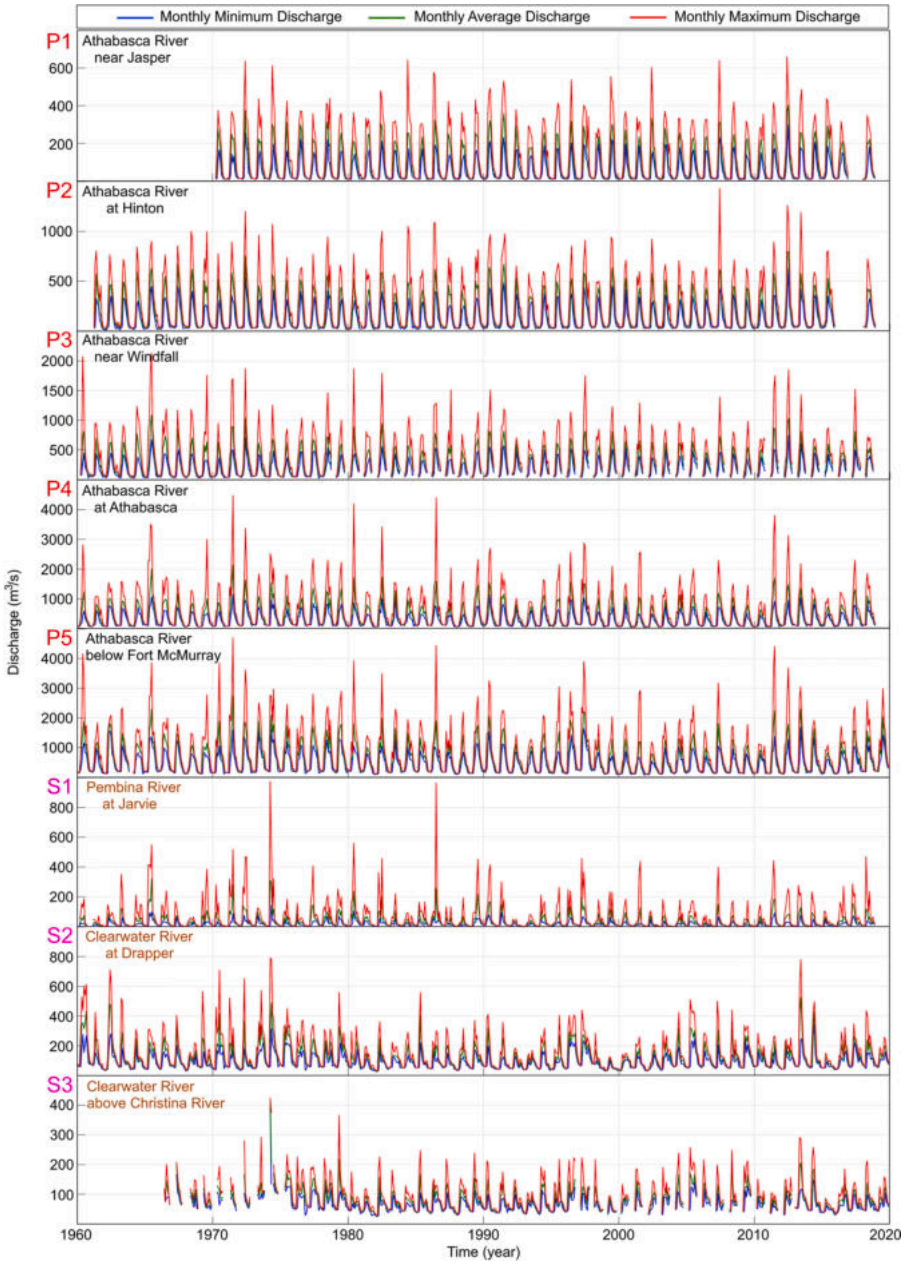

Fig. 5. The monthly hydrographs of the eight stations shown by stars in Fig. 1 since 1960.

values are missing, making the simple trend fit unrealistic. Similarly, the consistent data gaps from 1967 to 1976 and from 1997 to 2014 during winter for S3 significantly increased the estimated intercept via the simple fit that is less reliable compared to the simultaneous season-trend fit, see Fig. 10d and Table 3.

The gradual temperature increase by about 0.03 °C/a and annual precipitation decrease by about 1.5 mm/a in ARB are likely the main factors that have reduced the streamflow gradually since 1960 as listed in Table 3. The quadratic trend and seasonal components are also fitted to the discharge time series for P4 and P5, but the results show almost the same decreasing rate in streamflow since 1960. Only the linear trend results are shown herein to provide an overall estimate for changing streamflow since 1960. Note that the overall decreasing or increasing linear trend since 1960 may not however be a reliable forecast for the mid and late 21st century.

Figures 9 and 10 also show ALLSSs and LSWSs of each time series. From the amplitude spectra and spectrograms, one can see that the annual components have the highest amplitudes in all the eight discharge time series. The semi-annual components followed by the higher frequency components have more amplitude variability over time for all the eight time series. Fig. 9b shows higher amplitude for the semi-annual component since 1979. This is mainly due to the presence of consistent data gaps during the winter since 1979

where the presumably lower and flatter discharge values are missing, similarly for Fig. 10d, see the Supplementary Materials for more details (Slater and Villarini, 2016; Ghaderpour and Vujadinovic, 2020b).

Jumps in the trend component of a hydrological time series may occur due to various events, such as floods and drought, and human-induced changes, including urbanization, deforestation, and water diversions (Farsi et al., 2020). To investigate whether there are any significant jumps in the trend component of the time series, JUST is applied to estimate the jump locations in the trend component of each time series by allowing them to be at least a decade apart. The estimated trend results are illustrated in Fig. 11. The most significant jumps are detected for P4 and P5 in April 1971, May 1989, and April 2011, see the black and blue broken lines. As

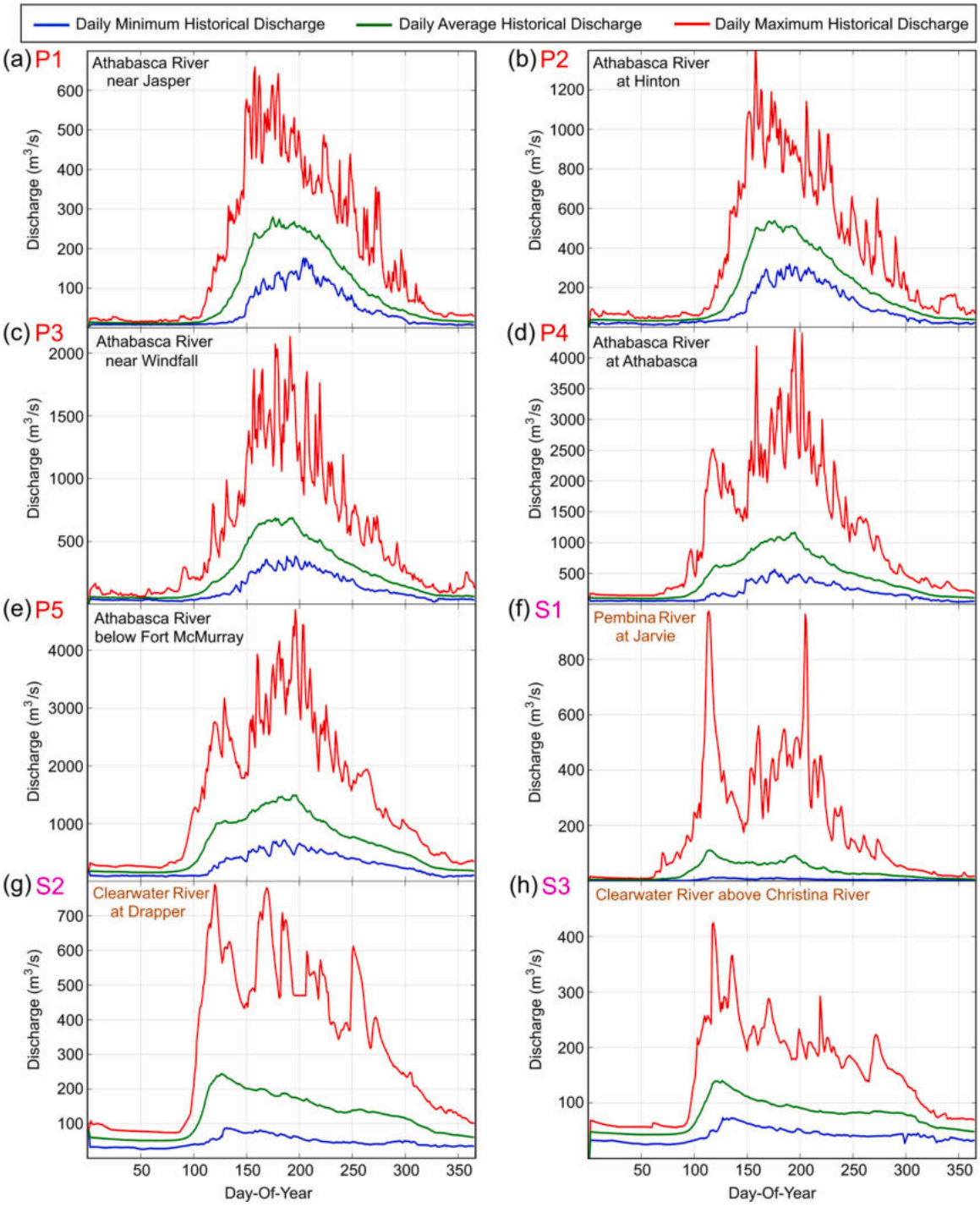

Fig. 6. The sixty-year hydrographs of the eight stations shown by stars in Fig. 1.

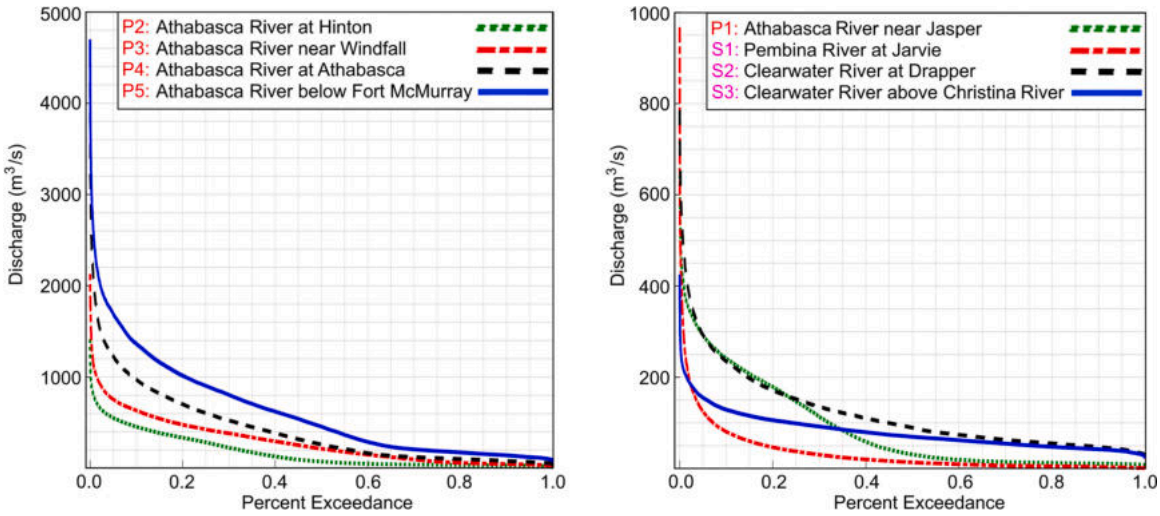

Fig. 7. Flow duration curves for the historical discharge time series since 1960. (For interpretation of the references to color in the text, the reader is referred to the web version of this article.)

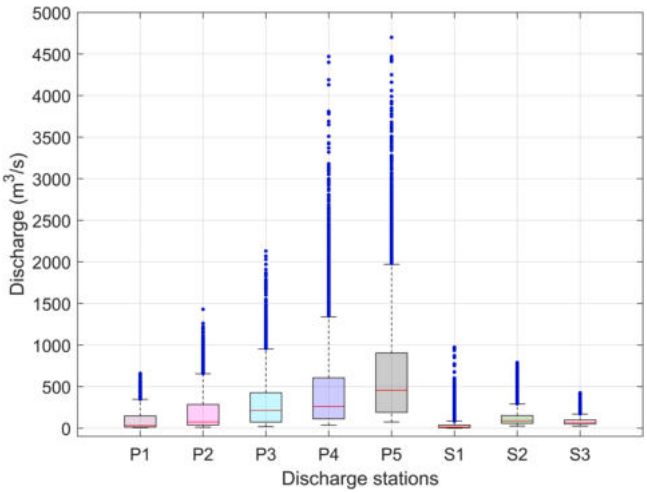

Fig. 8. The box plots of the historical discharges measured at the eight stations, shown in Fig. 1, since 1960. The blue circles are the outliers. (For interpretation of the references to color in this figure legend, the reader is referred to the web version of this article.)

listed in Table 3, the estimated trends for the entire time series show gradual reductions in discharge values except for P1.

3.3. Coherency analysis

To see how the flow fluctuation at Athabasca (P4) impacts the flow below Fort McMurray (P5), LSCSA and LSCWA are applied to their corresponding discharge time series, and the results are demonstrated in Fig. 12. The white arrows displayed on LSCWSs represent the phase differences between the components of the first (P5) and the second (P4) time series, following the trigonometric circle principle. The top LSCWS shows strong coherency between the annual components of both discharge time series with an overall phase difference of -2 degrees estimated by LSCSA, which indicates that the amplitude of the annual component for P5 reaches its maximum about two days after the one for P4. The bottom LSCS and LSCWS in Fig. 12 are obtained by suppressing the annual peaks, i.e., by removing the annual components while considering their removal effects in the residual series. Note that almost all the arrows displayed on the most coherent components are pointing to the southeast (falling in the fourth quadrant), meaning that the components of the time series for P4 lead the ones for P5. For the arrows, as an example, note that an angle of ± 14 degrees at 10 cycles/year is equivalent to an angle of ± 2 degrees at 1 cycle/year when converted to time (both means about two days lag/lead).

Toward the Athabasca River path from Athabasca (P4) to Fort McMurray (P5), many streams in the nearby subbasins flow into the Athabasca River and result in an increase in the flow at P5 as compared to P4. One of the main sources of the discrepancy in the

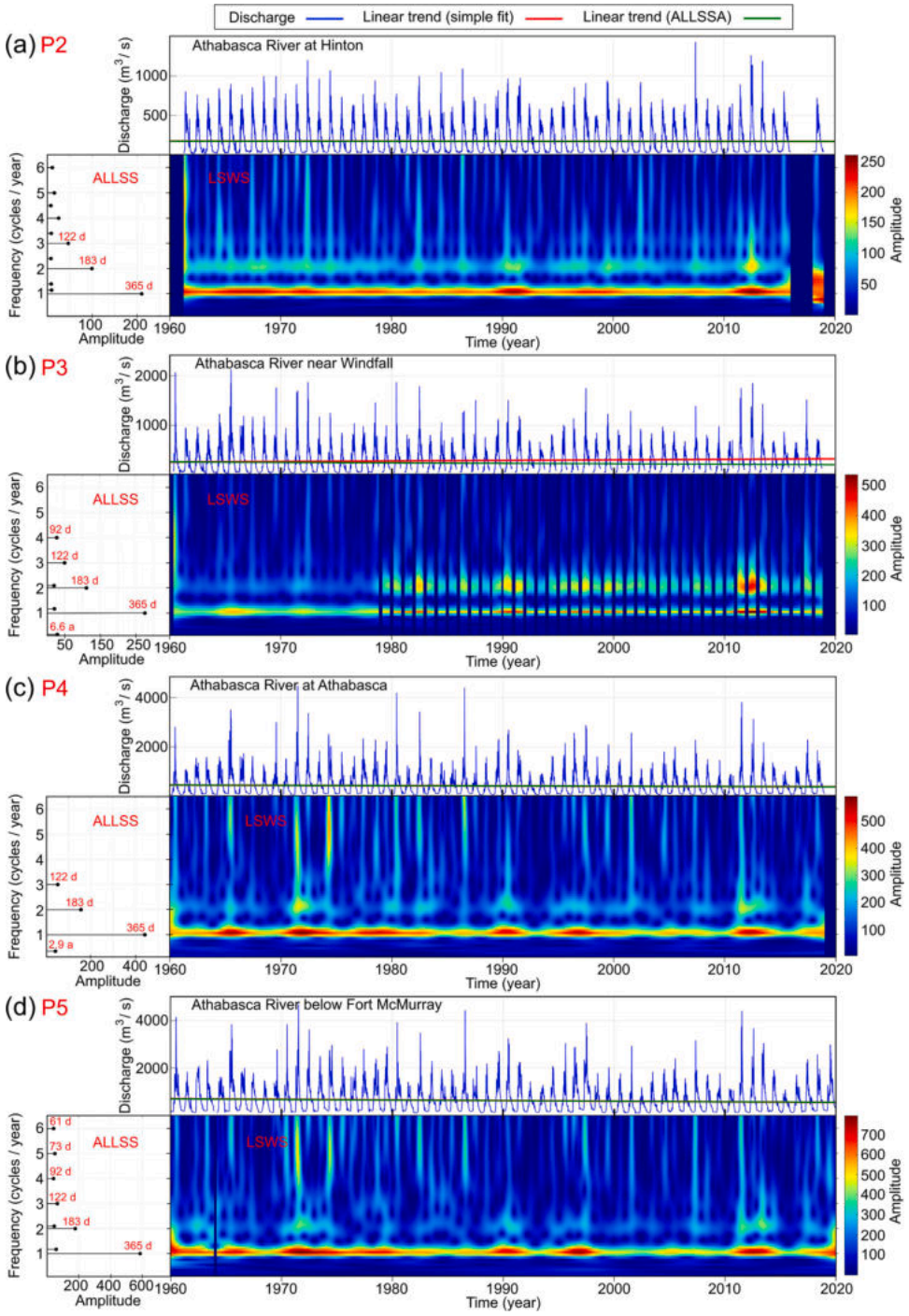

Fig. 9. Discharge time series along with the linear trend fits whose intercepts and slopes are listed in Table 3 and their corresponding ALLSS and LSWS. (For interpretation of the references to color in the text, the reader is referred to the web version of this article.)

discharge values measured at P4 and P5 is the water flowing into the Athabasca River from the Clearwater River (S2). From the bottom left panel in Fig. 2, the means of the annual precipitation time series are almost the same across the northern region, and so the coherency analysis between the discharge time series at P5 and the precipitation time series for the northern region is generally a logical approach.

Figure 13 shows the LSCSA and LSCWA of these two time series. From the cross-spectrograms, one can observe that the seasonal components are coherent, in particular the annual and semi-annual components. The annual and semi-annual components of the

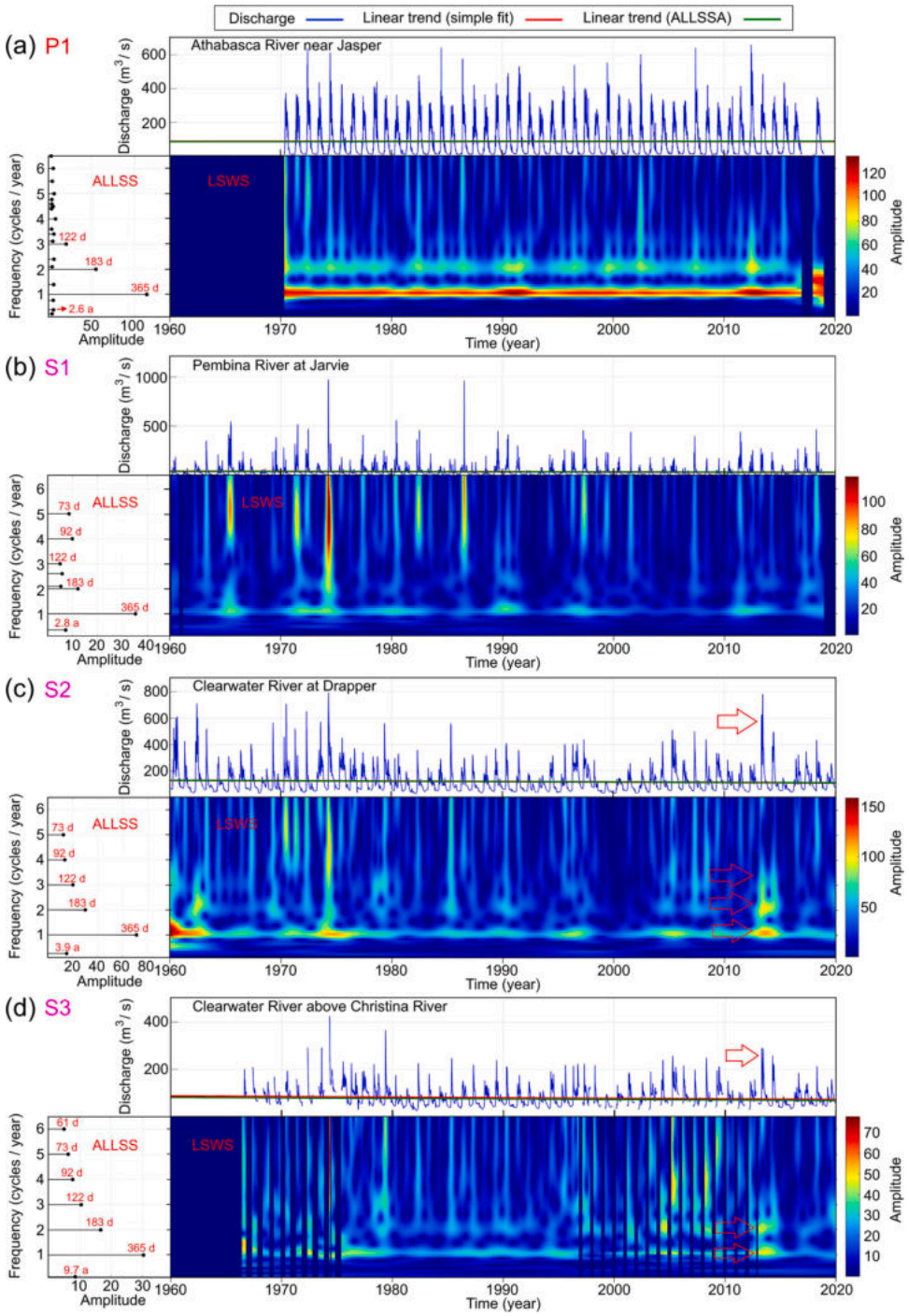

Fig. 10. Discharge time series with the linear trend fits whose intercepts and slopes are listed in Table 3 and their ALLSS and LSWS. The arrows show the impact of a flood event on the series and spectrograms. (For interpretation of the references to color in the text, the reader is referred to the web version of this article.)

precipitation time series generally lead the ones in the discharge time series by a few days. From the direction of the arrows, the phase differences at the higher frequencies are up to several days. For example, the single arrow displayed at 11.8 cycles/year (one month) in 2005 in the top LSCWS, has an angle of $\psi = -94$ degrees, meaning that the monthly component of the precipitation time series in 2005 leads the one in the discharge time series by about eight days. The bottom LSCS and LSCWS are obtained by suppressing the annual

Table 3
The estimated intercepts and slopes of the linear trends for the eight discharge time series shown in Figs. 9 and 10.

Station	Intercept (simple fit)	Slope (simple fit)	Intercept (ALLSSA)	Slope (ALLSSA)
P1	86.6160 ± 1.5220	0.0000 ± 0.0552	85.2898 ± 0.6118	0.0431 ± 0.0222
P2	175.7253 ± 2.6031	-0.0658 ± 0.0807	174.1958 ± 1.0657	-0.0318 ± 0.0331
P3	257.5546 ± 3.5614	1.1019 ± 0.1120	260.1937 ± 1.7889	-0.9446 ± 0.0603
P4	453.6464 ± 5.6836	-1.1615 ± 0.1669	453.9887 ± 3.4044	-1.1690 ± 0.0999
P5	699.0171 ± 7.3652	-2.5314 ± 0.2119	692.2286 ± 4.1997	-2.3807 ± 0.1208
S1	38.6457 ± 0.7687	-0.1911 ± 0.0226	37.6001 ± 0.6550	-0.1612 ± 0.0192
S2	129.3884 ± 1.2044	-0.3138 ± 0.0348	129.8871 ± 0.9056	-0.3211 ± 0.0261
S3	86.5433 ± 0.6559	-0.2452 ± 0.0209	80.8379 ± 0.4853	-0.2162 ± 0.0153

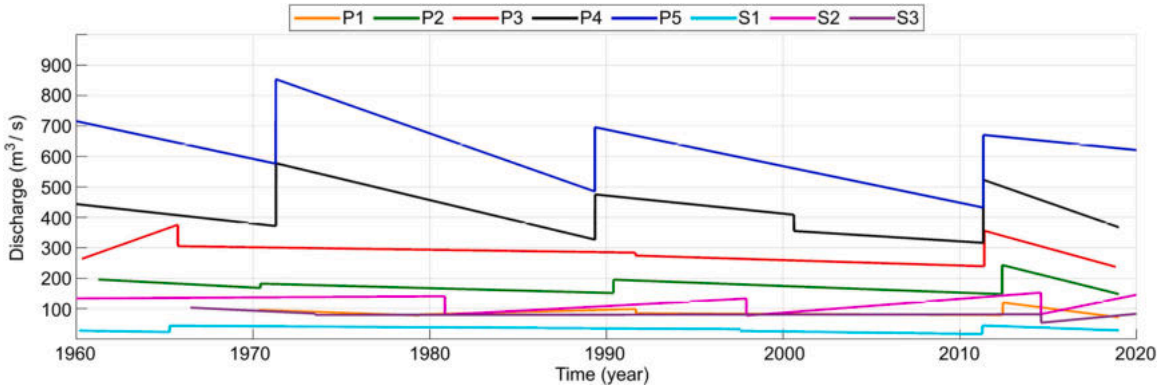

Fig. 11. Detected jumps in the trend component for the eight discharge time series using JUST with sliding windows whose sizes cover approximately three years of data.

peaks from both time series. The percentage variances between the annual and semi-annual components in Fig. 13 are less than the ones shown in Fig. 12, indicating comparatively lower coherency (see the maximum of 8% and 4% vs. 50% and 25% in the color bars). LSCWA can also be applied to the discharge and precipitation time series corresponding to each subbasin to investigate the coherency and phase differences more accurately.

4. Discussion

The spectral and wavelet analyses presented herein did not require any interpolation, gap-filling, and de-spiking of the original measurements, highlighting one of the main advantages of LSWAVE as compared to CWT and XWT (Ghaderpour et al., 2018a). The spectrograms showed significantly higher annual and semi-annual amplitudes in the early 1970s, 1990s, and 2010s for all the eight time series, in particular for P1 to P5. The high amplitude peaks in the spectrograms shown in Figs. 9 and 10 may correspond to the historical flood events. For example, in June 2013, ARB experienced a significant and devastating flood event on the Hangingstone and Clearwater Rivers upstream of Fort McMurray, mainly as a result of ice jams, heavy rainfall, and subsequent high flows in the Hagingstone River according to the reports by the Government of Alberta. The impact of this flood event on the discharge time series and their corresponding spectrograms can be observed in Fig. 10c and d (see the red arrows) and consequently in Fig. 9d. For forecasting purposes, one may expect to see similar seasonal amplitudes in the early 2030s provided that other conditions impacting the flow will not drastically change. Such pattern cannot be observed in LSSA or ALLSSA because their results are only in the frequency domain not in the time-frequency domain.

Segmentation allows a better fit of harmonics and linear trend to the series especially when the time series has components with variability of frequency and amplitude over time. Of course, quadratic and cubic trends may also be used in JUST, however, as a simple estimate for the rate of change of flow over decades, the linear trend is considered herein. The JUST results illustrated in Fig. 11 also showed significant jumps in the trend component of discharge series for P4 and P5 (with relatively higher drainage areas) around years 1970, 1990, and 2010, and so one may expect to observe a significant jump in the early 2030s for the flow at P4 and P5 as well.

From LSCSA and LSCWA, the precipitation and temperature were found to be two of the main drivers of the streamflow fluctuation for ARB. Unlike the correlation analysis that shows a possible relationship between climate and flow values, the coherency analysis shows how the signals are coherent in the frequency or time-frequency domain that along with the phase difference information provides a more robust result. For example, Fig. 13 showed that the coherent annual, semi-annual, and higher frequency signals of the daily-precipitation generally lead the ones in the streamflow. Providing such phase relationship between the components of both time series is extremely helpful in forestry, precision agriculture, and streamflow forecasting. Note that the variances of coherent signals were below 10%, that shows other factors, such as vegetation and soil moisture, may have also significantly impacted the streamflow.

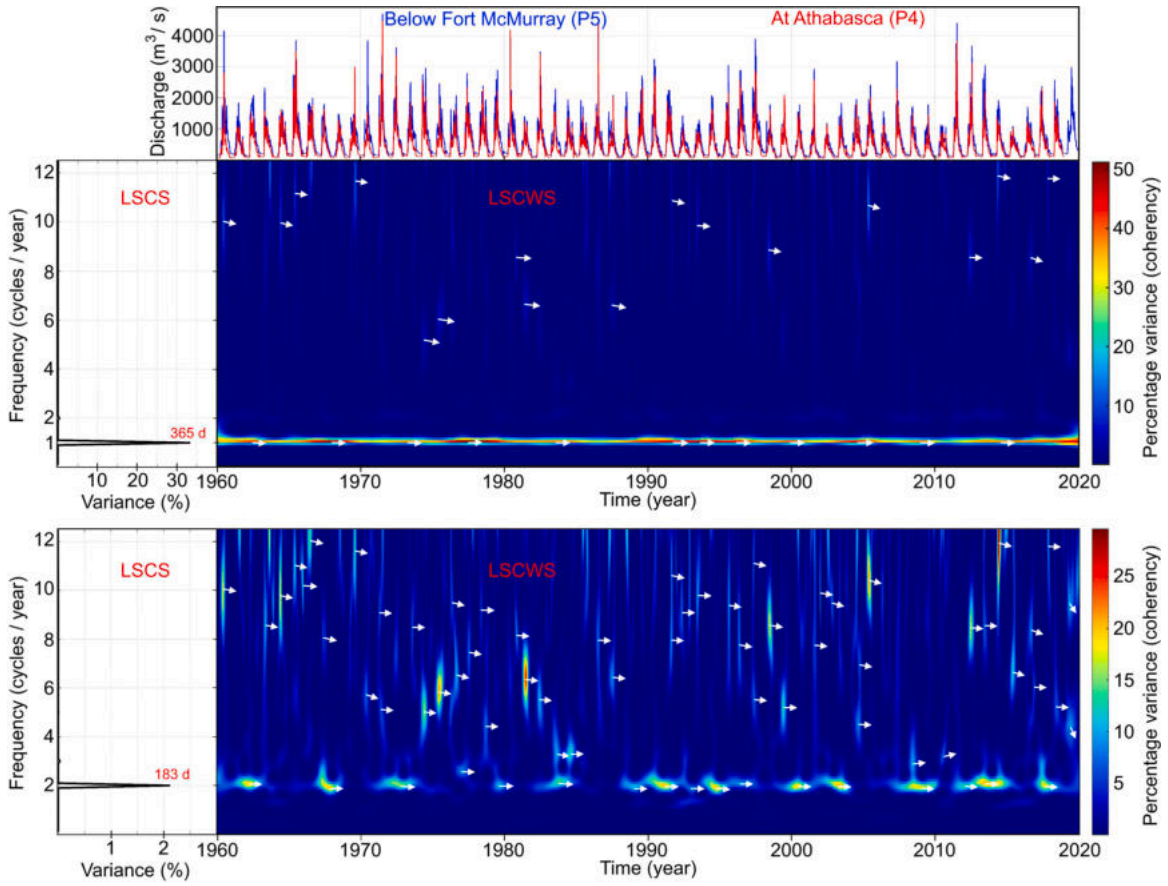

Fig. 12. The coherency analyses between the two discharge time series: Below Fort McMurray (P5) and At Athabasca (P4). The bottom LSCS and LSCWS panels are obtained by simultaneously suppressing the trend and annual cycles. The arrows display the phase differences between the most significant coherent components within localized time-frequency neighborhoods. Arrows pointing to the right, left, up, and down mean in-phase, out-of-phase, P5 leads, and P4 leads, respectively.

The results herein showed that the mean temperature of ARB has increased by about 2 °C since 1960. The mean temperature is projected to increase by approximately 2 °C for the mid-century (2021–2060) that is consistent with the observations made by Leong and Donner (2015) and Shrestha et al. (2017). Eum et al. (2017) used the ensemble mean of several GCMs and reported an increase of 7–10% mean annual precipitation in ARB during the mid-century. Therefore, due to increased snowmelt as the result of temperature increase, one may expect that the blue water increases during the mid-century in ARB (Shrestha et al. 2017). However, this may also decrease the snowpack volume for the spring freshet. As for the streamflow simulation, one would expect wider left tail for the asymmetric Gaussian function, demonstrated in Supplementary Fig. 3. From the recurring patterns of spectral peaks in the spectrograms shown in Figs. 10 and 11, one may deduce that the water resources in ARB may increase in 2030s which somewhat agrees with the observations made by Shrestha et al. (2017). The lower elevated regions of ARB, e.g., below Fort McMurray, may also experience a substantial increase in spring season blue water yield.

Since about 82% of the region is forested, one may investigate the relationships between the precipitation and plant root mechanism and water absorption via coherency analysis of satellite data to get an insight on how much delay is expected for a change to occur in streamflow after precipitation, particularly crucial for forecasting and mitigating drought and flood (Strong and La Roi, 1983; Xu et al., 2019; Ghaderpour and Vujadinovic, 2020b). Inverse modeling methods are not usually related to any control equations, such as Richards' equation (Richards, 1931). Streamflow is one of key hydrological parameters, which is very complex in nature, depending on soil types, vegetation, topology, and weather condition. LSWA results presented herein have only shown how the seasonal component of the streamflow has changed over time while the LSCWA has shown the possible coherency between the components of climate and streamflow time series.

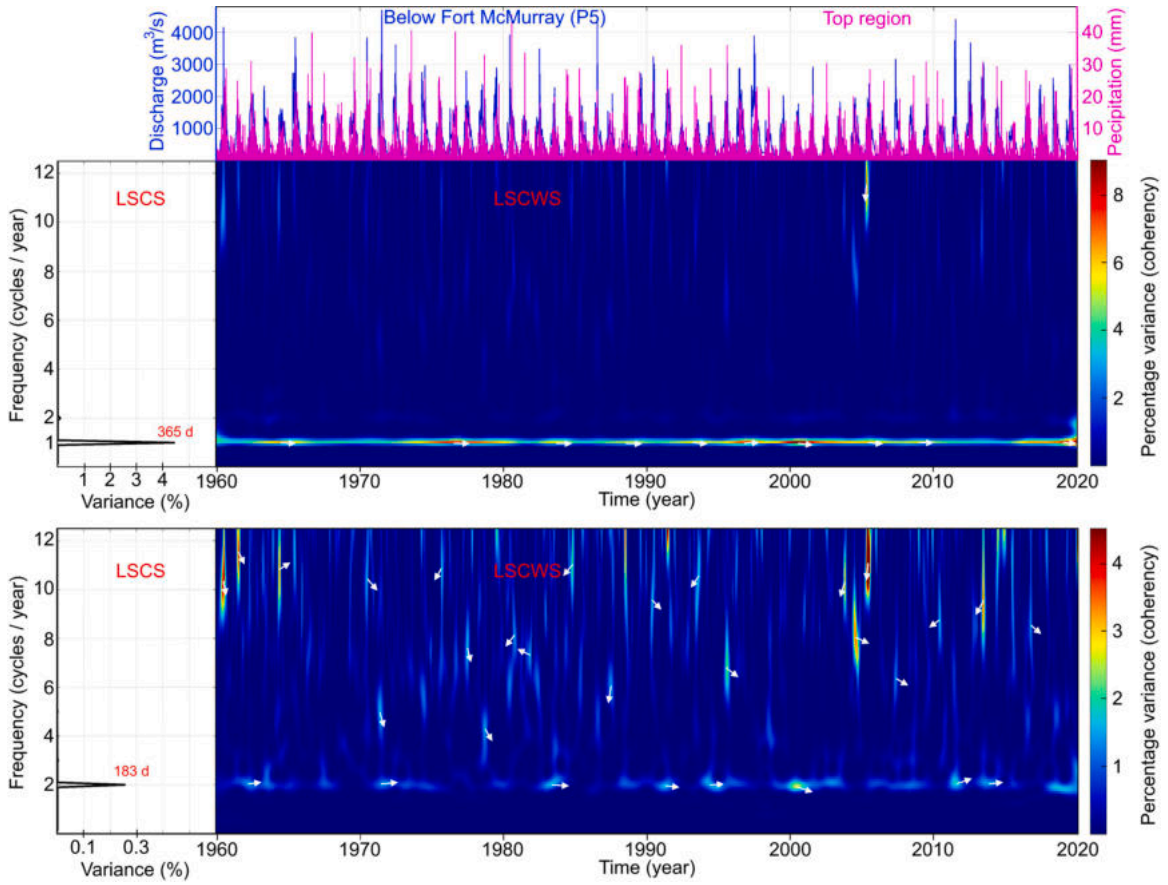

Fig. 13. The coherency analyses between the discharge time series for the Athabasca River below Fort McMurray (P5) and the daily-precipitation for the northern region shown in Fig. 1. The arrows display the phase differences between the most significant coherent components within localized time-frequency neighborhoods. The bottom LSCS and LSCWS panels are obtained by simultaneously suppressing the trend and annual cycles. Arrows pointing to the right, left, up, and down mean in-phase, out-of-phase, discharge leads, and precipitation leads, respectively.

5. Conclusions

In this contribution, the sixty-year-long streamflow, temperature, and precipitation time series for ARB were analyzed using several methods, where each method provided certain and useful information. Although traditional tools, such as box plots, hydrographs, and flow-duration curves provide specific information about the hydrological data, they cannot clearly show the components of the data and how they change over time. For example, from the flow-duration curves illustrated in Fig. 7, it is predicted that the probability that streamflow exceeds 1000 m^3/s along the Athabasca River is less than 0.2 during the mid-century. Furthermore, these tools cannot be used to investigate how climate change influences the streamflow because they provide no phase information and no coherency/correlation. On the other hand, wavelet and cross-wavelet analyses clearly show how the components of the data change over time and how climate change may impact the streamflow over time.

The trend analyses showed gradual changes in the time series values. The simultaneous season-trend fit using the spectral analysis showed more reliable results for estimating the trend component of the discharge time series as compared to the traditional regression method (simple fit), especially for unequally spaced time series with data gaps. The spectral analysis provided the amplitudes and frequencies of the inter- and intra-annual components while the spectrograms also showed amplitude variability of these components over time. All the eight streamflow time series showed statistically significant annual and semi-annual components with variability of amplitudes over time as well as other short-duration high-frequency components that were linked to the climate change via the coherency analyses. From the recurring patterns in the spectrograms and trend results, it is projected that the blue water resources may increase during the mid-century, in particular below Fort McMurray.

Therefore, it is crucial for hydrological and climate studies to consider seasonal variations along with gradual changes in the ecology and hydrology of watersheds. It is expected that such spectral and wavelet analyses can also help to provide more reliable

climate and hydrological forecasts. As demonstrated in the Supplementary Materials, LSWAVE can estimate the trend and seasonal components more accurately than the traditional regression analysis and CWT without any need for interpolation and repairing the data. The tools in the LSWAVE and JUST software packages can also estimate the signals more accurately by considering the observational uncertainties.

Limitations of this study include: (1) the proposed spectral and wavelet methods were only applied to discharge and climate data without considering other factors, such as soil profile, topology, and vegetation, and (2) the analyses of discharge time series were shown for only eight hydrometric stations near and along the Athabasca River with relatively large drainage areas and sufficiently long historical data.

Abbreviations

ALLSSA	Anti-Leakage Least-Squares Spectral Analysis
ALLSS	Anti-Leakage Least-Squares (Amplitude) Spectrum
ARB	Athabasca River Basin
CWT	Continuous Wavelet Transform
GCM	Global Climate Model
GIS	Geographic Information System
JUST	Jumps Upon Spectrum and Trend
LSCSA	Least-Squares Cross-Spectral Analysis
LSCS	Least-Squares Cross-Spectrum
LSCWA	Least-Squares Cross-Wavelet Analysis
LSCWS	Least-Squares Cross-Wavelet Spectrogram
LSSA	Least-Squares Spectral Analysis
LSS	Least-Squares Spectrum
LSWA	Least-Squares Wavelet Analysis
LSWS	Least-Squares Wavelet (Amplitude) Spectrogram
LSWAVE	Least-Squares Wavelet – Software
TIN	Triangulated Irregular Network
XWT	Cross-Wavelet Transform

CRediT authorship contribution statement

Ebrahim Ghaderpour: Conceptualization, Data curation, Methodology, Formal analysis, Writing – original draft, Visualization, Writing – review & editing. **Tijana Vujadinovic**: Conceptualization, Visualization, Writing – review & editing. **Quazi K. Hassan:** Conceptualization, Visualization, Writing – review & editing.

Declaration of Competing Interest

The authors report no declarations of interest.

Acknowledgments

The authors acknowledge the Government of Canada (Water Survey of Canada) and the Government of Alberta (Alberta Agriculture and Forestry) for providing the water discharge and gridded climate data for non-commercial/research purposes free of cost. The authors sincerely thank the editors and reviewers for their comprehensive comments that significantly helped to improve the presentation of the paper.

Appendix A. Supplementary data

Supplementary data associated with this article can be found, in the online version, at https://doi.org/10.1016/j.ejrh.2021.100847.

References

Azuara, J., Sabatier, P., Lebreton, V., Jalali, B., Sicre, M.A., Dezileau, L., Bassetti, M.A., Frigola, J., Combourieu-Nebout, N., 2020. Mid- to Late-Holocene Mediterranean climate variability: Contribution of multi-proxy and multi-sequence comparison using wavelet spectral analysis in the northwestern Mediterranean basin. Earth-Sci. Rev. 208, 103232.

Bawden, A.J., Linton, H.C., Burn, D.H., Prowse, T.D., 2014. A spatiotemporal analysis of hydrological trends and variability in the Athabasca River region, Canada. J. Hydrol. 509, 333–342.

Craymer, M.R., 1998. The Least-Squares Spectrum, Its Inverse Transform and Autocorrelation Function: Theory and Some Application in Geodesy. University of Toronto, Canada. PhD Diss.

Dibike, Y., Eum, H.I., Prowse, T., 2018. Modelling the Athabasca watershed snow response to a changing climate. J. Hydrol.: Reg. Stud. 15, 134–148.
Du, X., Shrestha, N.K., Wang, J., 2019. Assessing climate change impacts on stream temperature in the Athabasca River Basin using SWAT equilibrium temperature model and its potential impacts on stream ecosystem. Sci. Total Environ. 650 (2), 1872–1881.
Eum, H.I., Gupta, A., 2019. Hybrid climate datasets from a climate data evaluation system and their impacts on hydrologic simulations for the Athabasca River Basin in Canada. Hydrol. Earth Syst. Sci. 23, 5151–5173.
Eum, H.I., Dibike, Y., Prowse, T., 2017. Climate-induced alteration of hydrologic indicators in the Athabasca River Basin, Alberta, Canada. J. Hydrol. 544, 327–342.
Fang, Z., Bogena, H.R., Kollet, S., Koch, J., Vereecken, H., 2015. Spatio-temporal validation of long-term 3D hydrological simulations of a forested catchment using empirical orthogonal functions and wavelet coherence analysis. J. Hydrol. 529 (3), 1754–1767.
Farsi, N., Mahjouri, N., Ghasemi, H., 2020. Breakpoint detection in non-stationary runoff time series under uncertainty. J. Hydrol. 590, 125458.
Foster, G., 1996. Wavelet for period analysis of unevenly sampled time series. Astron. J. 112 (4), 1709–1729.
Foster, H.A., 1934. Duration curves. Trans. ASCE 99, 1213–1267.
Ghaderpour, E., 2021. JUST: MATLAB and Python software for change detection and time series analysis. GPS Solut. 25, 85.
Ghaderpour, E., Vujadinovic, T., 2020a. Change detection within remotely-sensed satellite image time series via spectral analysis. Remote Sens. 12 (23), 4001.
Ghaderpour, E., Vujadinovic, T., 2020b. The potential of the least-squares spectral and cross-wavelet analyses for near-real-time disturbance detection within unequally spaced satellite image time series. Remote Sens. 12 (15), 2446.
Ghaderpour, E., Pagiatakis, S.D., 2019. LSWAVE: a MATLAB software for the least-squares wavelet and cross-wavelet analyses. GPS Solut. 23, 50.
Ghaderpour, E., 2018. Least-Squares Wavelet Analysis and Its Applications in Geodesy and Geophysics. York University, Canada. PhD Diss.
Ghaderpour, E., Ince, E.S., Pagiatakis, S.D., 2018a. Least-squares cross-wavelet analysis and its applications in geophysical time series. J. Geod. 92 (10), 1223–1236.
Ghaderpour, E., Liao, W., Lamoureux, M.P., 2018b. Antileakage least-squares spectral analysis for seismic data regularization and random noise attenuation. Geophysics 83 (3), V157–V170.
Ghaderpour, E., Pagiatakis, S.D., 2017. Least-squares wavelet analysis of unequally spaced and non-stationary time series and its applications. Math. Geosci. 49 (7), 819–844.
Graf, A., Bogena, H.R., Drüe, C., Hardelauf, H., Pütz, T., Heinemann, G., Vereecken, H., 2014. Spatiotemporal relations between water budget components and soil water content in a forested tributary catchment. Water Resour. Res. 50 (6), 4837–4857.
Grinsted, A., Moore, J.C., Jevrejeva, S., 2004. Application of the cross wavelet transform and wavelet coherence to geophysical time series. Nonlinear Process. Geophys. 11, 561–566.
Hwang, H.T., Park, Y.J., Sudicky, E.A., Berg, S.J., McLaughlin, R., Jones, J.P., 2018. Understanding the water balance paradox in the Athabasca River Basin, Canada. Hydrol. Process. 32 (6), 729–746.
Kundzewicz, Z.W., Robson, A.J., 2004. Change detection in hydrological records-a review of the methodology /Revue methodologique de la detection de changements dans les chroniques hydrologiques. Hydrol. Sci. J. 49 (1), 7–19.
Labat, D., 2008. Wavelet analysis of the annual discharge records of the world's largest rivers. Adv. Water Resour. 31, 109–117.
Leong, D.N.S., Donner, S.D., 2015. Climate change impacts on streamflow availability for the Athabasca Oil Sands. Climate Change 133 (4), 651–663.
Liu, H., Yu, Y., Zhao, W., Guo, L., Liu, J., Yang, Q., 2020. Inferring subsurface preferential flow features from a wavelet analysis of hydrological signals in the Shale Hills catchment. Water Resour. Res. 56 (11), 21.
Li, M., Shao, Q., Zhang, L., Chiew, F.H.S., 2010. A new regionalization approach and its application to predict flow duration curve in ungauged basins. J. Hydrol. 398 (1–2), 137–145.
Lomb, N.R., 1976. Least-squares frequency analysis of unequally spaced data. Astrophys. Space Sci. 39, 447–462.
McGill, R., Tukey, J., Larsen, W., 1978. Variations of box plots. Am. Stat. 32 (1), 12–16.
Mallat, S., 1999. A Wavelet Tour of Signal Processing. Academic Press, Cambridge UK.
Mitas, L., Mitasova, H., 1999. Spatial interpolation. In: Longley, P.A., Rhind, D.W., Goodchild, M.F., Maguire, D.J. (Eds.), Geographical Information Systems: Principles, Techniques, Management and Applications. John Wiley & Sons, Chichester, pp. 481–492.
Pagiatakis, S., 1999. Stochastic significance of peaks in the least-squares spectrum. J. Geod. 73 (2), 67–78.
Payne, J.T., Wood, A.W., Hamlet, A.F., Palmer, R.N., Lettenmaier, D.P., 2004. Mitigating the effects of climate change on the water resources of the Columbia River basin. Clim. Change 62 (1–3), 233–256.
Richards, L.A., 1931. Capillary conduction of liquids through porous mediums. Physics 1 (5), 318–333.
Ruan, X., Qiu, F., Dyck, M., 2016. The effects of environmental and socioeconomic factors on land-use changes: a study of Alberta, Canada. Environ. Monit. Assess. 188, 446.
Rudi, J., Pabel, R., Jager, G., Koch, R., Kunoth, A., Bogena, H., 2010. Multiscale analysis of hydrologic time series data using the Hilbert-Huang transform. Vadose Zone J. 9 (4), 925–942. https://doi.org/10.2136/vzj2009.0163.
Schultea, J.A., Najjar, R.G., Li, M., 2016. The influence of climate modes on streamflow in the Mid-Atlantic region of the United States. J. Hydrol.: Reg. Stud. 5, 80–99.
Shrestha, N.K., Wang, J., 2018. Predicting sediment yield and transport dynamics of a cold climate region watershed in changing climate. Sci. Total Environ. 635, 1030–1045.
Shrestha, N.K., Du, X., Wang, J., 2017. Assessing climate change impacts on fresh water resources of the Athabasca River Basin, Canada. Sci. Total Environ. 601, 425–440.
Slater, L., Villarini, G., 2016. On the impact of gaps on trend detection in extreme streamflow time series. Int. J. Climatol. 37 (10), 3976–3983.
Strong, W.L., La Roi, G.H., 1983. Root-system morphology of common boreal forest trees in Alberta, Canada. Can. J. Forest Res. 13, 1164–1173.
Tibshirani, R., 1996. Regression shrinkage and selection via the lass. J. R. Stat. Soc. Ser. B (Methodol.) 58, 267–288.
Torrence, C., Compo, G.P., 1998. A practical guide to wavelet analysis. Bull. Am. Meteorol. Soc. 79 (1), 61–78.
Vaníček, P., 1969. Approximate spectral analysis by least-squares fit. Astrophys. Space Sci. 4, 387–391.
Vogel, R.R., Fennessey, N.W., 1994. Flow-duration curve. I: New interpretation and confidence intervals. J. Water Resour. Plan. Manag. 120 (4), 485–504.
Xu, Y., Yu, L., Cai, Z., Zhao, J., Peng, D., Li, C., Lu, H., Yu, C., Gong, P., 2019. Exploring intra-annual variation in cropland classification accuracy using monthly, seasonal, and yearly sample set. Int. J. Remote Sens. 40 (23), 8748–8763.
Zhu, Z., Woodcock, C.E., Holden, C., Yang, Z., 2015. Generating synthetic Landsat images based on all available Landsat data: predicting Landsat surface reflectance at any given time. Remote Sens. Environ. 162, 67–83.